Anatomy of the dielectric behavior of methyl-*m*-toluate glasses during and after vapor deposition ⊘

R. Richert ✉ (iD) ; M. E. Tracy (iD) ; A. Guiseppi-Elie (iD) ; M. D. Ediger (iD)

Check for updates

CrossMark

View Online

Export Citation

AIP Publishing

Anatomy of the dielectric behavior of methyl-*m*-toluate glasses during and after vapor deposition

View Online   Export Citation   CrossMark

R. Richert,[1,a] ⓘ M. E. Tracy,[2] ⓘ A. Guiseppi-Elie,[3] ⓘ and M. D. Ediger[2] ⓘ

AFFILIATIONS

[1] School of Molecular Sciences, Arizona State University, Tempe, Arizona 85287, USA
[2] Department of Chemistry, University of Wisconsin-Madison, Madison, Wisconsin 53706, USA
[3] Department of Electrical and Computer Engineering, Texas A & M University, College Station, Texas 77843, USA

[a] Author to whom correspondence should be addressed: ranko@asu.edu

ABSTRACT

Glassy films of methyl-*m*-toluate have been vapor deposited onto a substrate equipped with interdigitated electrodes, facilitating *in situ* dielectric relaxation measurements during and after deposition. Samples of 200 nm thickness have been deposited at rates of 0.1 nm/s at a variety of deposition temperatures between 40 K and T_g = 170 K. With increasing depth below the surface, the dielectric loss changes gradually from a value reflecting a mobile surface layer to that of the kinetically stable glass. The thickness of this more mobile layer varies from below 1 to beyond 10 nm as the deposition temperature is increased, and its average fictive temperature is near T_g for all deposition temperatures. Judged by the dielectric loss, the liquid-like portion of the surface layer exceeds a thickness of 1 nm only for deposition temperatures above $0.8T_g$, where near-equilibrium glassy states are obtained. After deposition, the dielectric loss of the material positioned about 5–30 nm below the surface decreases for thousands of seconds of annealing time, whereas the bulk of the film remains unchanged.

Published under an exclusive license by AIP Publishing. https://doi.org/10.1063/5.0187166

I. INTRODUCTION

Cooling a supercooled liquid toward its glass transition temperature T_g is accompanied by a dramatic increase in the relaxation time. As T_g is approached, the relaxation time becomes ~1 s, but equilibration is still possible at typical cooling rates. Below T_g, cooling generates a driving force to densify and attain a low entropy/enthalpy state, but the time to reach equilibrium becomes prohibitively long. Remarkably, this kinetic limitation to equilibration below T_g can be circumvented. Swallen *et al.* have demonstrated that glasses of exceedingly high kinetic stability and density can be produced within minutes using physical vapor deposition (PVD),[1,2] whereas it may require thousands or millions of years of aging to arrive at a comparable state via cooling the liquid.[3,4] Experimental parameters that promote high kinetic stability are deposition temperatures around T_{dep} = $0.85T_g$ and deposition rates not exceeding r_{dep} = 1 nm s^{-1}.[5,6] Under those conditions, PVD is understood to combine the unusual situation of a low sub-

strate temperature, T_{dep}, with high mobility at the glass/vacuum interface.

Both the diffusivity and the relaxation time at the surface of organic liquids and glasses have been observed to be orders of magnitude faster than their respective bulk counterparts.[7–13] Estimates of the thickness of the mobile surface layer are based on studies of films and range from a few molecular layers to 20 nm,[8,11,14,15] with no indication of a significant difference between films obtained by vapor deposition and by cooling the liquid.[16] As a result of their high mobility, surface molecules are assumed to approach the equilibrium state effectively during PVD, unless buried too rapidly by subsequent deposition.[17,18] The extent of kinetic stability is thus determined by the competition between the surface relaxation time and the deposition rate, which determines the residence time of molecules near the surface.[19,20]

The higher density and kinetic stability of PVD glasses lead to a suppression of residual molecular mobility relative to glasses obtained by cooling the melt, and this is observable by dielectric

techniques as a reduction of the loss, ε'', or dissipation, $\tan\delta$.[21–23] Using high-resolution dielectric techniques, this study elucidates the structure and dynamics of glasses and liquids prepared by physical vapor deposition, both during and after the deposition process. To this end, we employ methyl-m-toluate (MMT), a molecular glass former with a glass transition temperature $T_g = 170$ K. MMT is simple in the sense that transforming the as-deposited glass to the supercooled liquid state above T_g recovers the properties achieved by cooling the melt. Note that some glasses fabricated by PVD fail to recover the expected liquid state after warming above T_g, e.g., 4-methyl-3-heptanol,[24] 2-methyltetrahydrofuran,[25] or butyronitrile.[26] We find that *in situ* dielectric measurements with a resolution of $\tan\delta = 10^{-7}$ provide a detailed picture of the film growth, the fictive temperature and thickness of the mobile surface layer, as well as the annealing behavior after deposition. The surface layer changes thickness from below 1 nm to more than 10 nm as the deposition temperature is increased from 100 to 170 K, and the changes observed in the course of annealing for 50 000 s are associated with the material near the surface.

II. EXPERIMENT

Methyl-m-toluate (MMT) has been purchased from Sigma-Aldrich and was used as received or after distillation, which gave the same results. A reservoir of MMT vapor was kept at pressures between 0.13 and 0.15 mbar, and the deposition rate was adjusted by a needle valve (Swagelok SS-SS4-KZ). Control of deposition time was through toggle valves, one before and one behind the needle valve. The sample was cooled using an evacuated Leybold RDK 12-320 closed-cycle helium refrigerator, and temperature was controlled with a Lakeshore Mod. 340 unit. Details of the deposition chamber have been provided in an earlier publication.[27] Samples were deposited onto one of two structures of a high precision microlithographically fabricated interdigitated electrode (IDE) cell, ABTECH IME 1050.5-FD-Au, with a borosilicate substrate.[28] Each capacitor consists of $n/2 = 50$ pairs of 100 nm thick gold fingers of $l = 5$ mm length, $w = 10$ μm width, and $s = 10$ μm digit spacing, but only one is used for the present experiments. The nominal geometric capacitance of the cell is $C_{geo} = \varepsilon_0 \times L/2 = 2.2$ pF, with $L = (s + w + l) \times (n - 1) = 49.55$ cm and ε_0 being the permittivity of vacuum. The periodicity of this structure is $\lambda = 2(s + w) = 40$ μm. The value of C_{geo} has been verified via calibration with 2-ethyl-1-hexanol at 295 K.

For typical vapor deposited films, the IDE capacitor is not completely filled on the z-axis, implying that the measured susceptibility χ_{app} remains below the actual susceptibility χ of the material. The case $\chi_{app} = \chi$ is achieved only for a film thickness $d \geq \lambda/2$, equivalent to a completely filled capacitor. Only for films with $d < 500$ nm does χ_{app} increase linearly with d, where $\chi_{app} = \chi \times d/(\lambda/8)$. Therefore, in order to gauge the thickness of a film via its capacitance increment $\chi_{app} C_{geo}$, the true value of χ needs to be determined by depositing a film of at least $\lambda/2 = 20$ μm thickness.

We have measured the capacitance, C, and dissipation, $\tan\delta$, during and after deposition onto the IDE using an ultraprecision capacitance bridge, the Andeen-Hagerling AH-2700A, set to a fixed frequency of $\nu = 1$ kHz, a frequency far above that of the dielectric loss peak for the glasses deposited here. The real part of
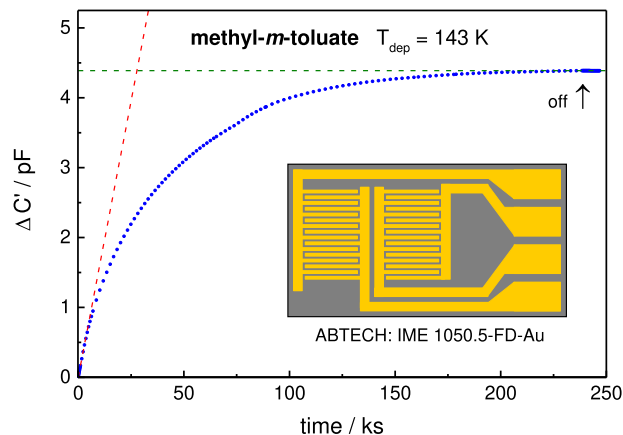

FIG. 1. MMT film deposited at $T_{dep} = 143$ K for >66 h at a rate in the range 0.1 nm/s $< r_{dep} < 0.2$ nm/s, leading to $d_{dep} > 20$ μm. The saturation capacitance increment is $\Delta C_{sat} = 4.4$ pF, thus $\chi_\infty = \Delta C_{sat}/C_{geo} = 2.0$. The capacitance is highly stable after deposition, losing only 1 fF in the subsequent 8000 s. The inset shows a schematic outline of the IMC cell used in this study.

the capacitance, C', is governed by ε_∞ and insensitive to the position, width, and amplitude of the dielectric relaxation profile. The imaginary part, C'', may reflect peak broadening or peak shifting to higher frequencies, both being qualitative indicators of higher mobility. As the dipole density remains practically constant, a significant change in overall dielectric amplitude, ε_s, is not expected to be significant. The apparent susceptibility $\Delta\chi_{app}$ of the sample is then determined via $\Delta\chi'_{app} = (C' - C'_{sub})/C_{geo}$ and $\Delta\chi''_{app} = (C'' - C''_{sub})/C_{geo}$, where $C' = C$, $C'' = C \times \tan\delta$, and C_{sub} represents the capacitance value prior to deposition, thus quantifying the substrate contribution. The subscript "app" denotes the apparent value of the susceptibility, which is the real $\Delta\chi$ multiplied by a filling factor $\varphi = d/(\lambda/8)$ that depends on the film thickness d, for $d \leq 500$ nm, and thus also on time, t, during the course of the deposition process. After deposition, the film thickness is determined via $d_{dep} = \chi'_{app}\lambda/(8\chi') = 5$ μm $\times (\chi'_{app}/\chi')$, where χ' is the calibration value obtained from a completely filled capacitor. The deposition rate is given by $r_{dep} = d_{dep}/t_{dep}$, with t_{dep} being the deposition time. Spectra of the sample in the liquid state are collected using a Solartron SI-1260 equipped with a calibrated DM-1360 transimpedance amplifier.

III. RESULTS

To be able to determine film thicknesses, the value of χ' in the glassy state is required, ideally obtained under conditions that replicate the preparation parameters of the other samples, $r_{dep} \approx 0.1$ nm s^{-1}. To this end, a sample is required that fills the capacitor completely, which was achieved after depositing for ~66 h, yielding a thickness of $d_{dep} > 20$ μm. The capacitance is saturated at $\Delta C_{sat} = 4.4$ pF so that $\chi_\infty = 2.0$ for the film is obtained (see Fig. 1).

A typical deposition process for a 200 nm film of MMT is depicted in Fig. 2, showing the linear increase of $\Delta\chi'$ expected for
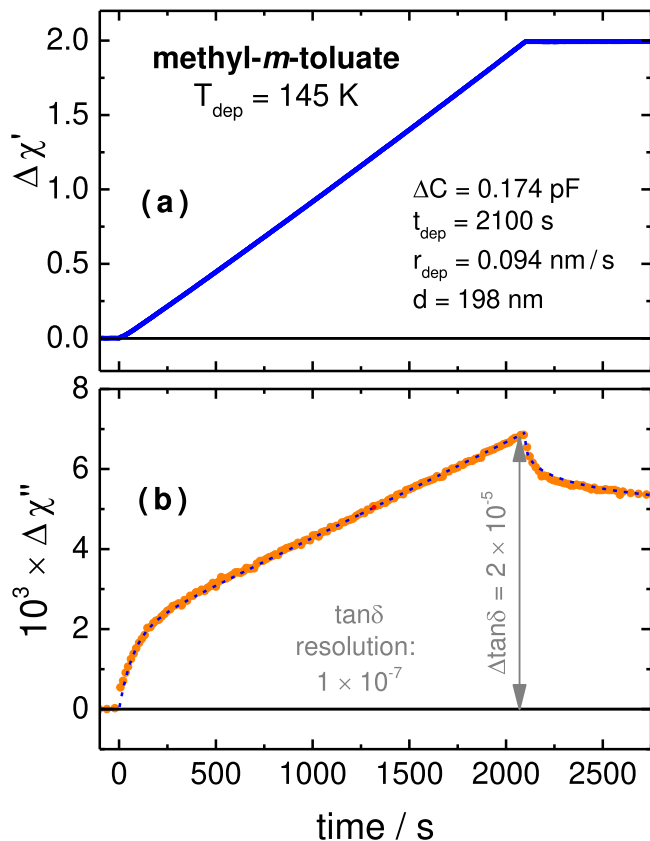
FIG. 2. Typical susceptibility increment during deposition of a 200 nm film of MMT at a rate of 0.094 nm/s. (a) Storage values are determined as $\Delta\chi'(t) = \Delta C'(t)/C_{geo} \times (\Delta C_{sat}/\Delta C)$, with $C_{geo} = 2.2$ pF and $\Delta C_{sat} = \chi_\infty \times C_{geo} = 4.4$ pF. ΔC is the capacitance increment at the end of deposition. (b) Loss values are calculated via $\Delta\chi''(t) = \Delta C''(t)/C_{geo} \times (\Delta C_{sat}/\Delta C)$. The arrow indicates the overall measured change in dissipation. $\Delta\tan\delta = 2 \times 10^{-5}$, with a resolution of 1×10^{-7}.

a constant deposition rate and a nonlinear rise of the loss, $\Delta\chi''$. This film is deposited at conditions for which a kinetically stable state is expected. Heating the MMT glass of Fig. 2 above $T_g = 170$ K and then measuring the loss spectra in the liquid state leads to the results shown in Fig. 3, which are corrected for the substrate contribution and scaled to represent what would be observed in a completely filled capacitor. The rise in amplitude upon warming is due to the slow transformation process from the stable glass to the liquid. The drop in amplitude for temperatures in excess of 190 K is the result of crystallization. The amplitudes and peak frequencies ν_{max} of Fig. 3 are consistent with bulk MMT cooled from the melt;[29] see the $\nu_{max}(T)$ traces in the inset of Fig. 3. In this range, the temperature dependence follows a Vogel–Fulcher–Tammann (VFT) relation, $\log_{10}(\tau_{max}/s) = A + B/(T - T_0)$, with $A = -26.14$, $B = 2640$ K, and $T_0 = 75.1$ K.

Physical vapor depositions and measurements such as the one depicted for $T_{dep} = 145$ K in Fig. 2 have been performed at temperatures from 100 to 170 K, with spacings of 10 K or less. In all cases, films of about $d_{dep} = 225 \pm 10$ nm thickness have been deposited using rates of $r_{dep} = 0.092 \pm 0.004$ nm s^{-1}, with a typical deposition
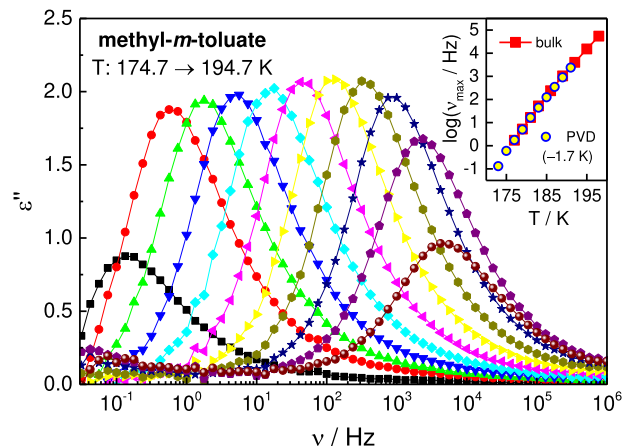

FIG. 3. Dielectric loss spectra ($\varepsilon'' = \chi''$, corrected and scaled) measured after the deposition process of Fig. 2 between $T = 174.7$ and 194.7 K from low to high temperatures in steps of 2 K. The loss profiles show the transformation from the stable glass to the liquid state as well as crystallization when the peak frequency exceeds 1 kHz. Otherwise, the profiles are consistent with the behavior of MMT cooled from the melt. The inset shows peak loss frequencies ν_{max} derived from the spectra of the main figure (open circles), compared with bulk MMT results (diamonds) taken from Ref. 29, after a temperature shift of -1.7 K.
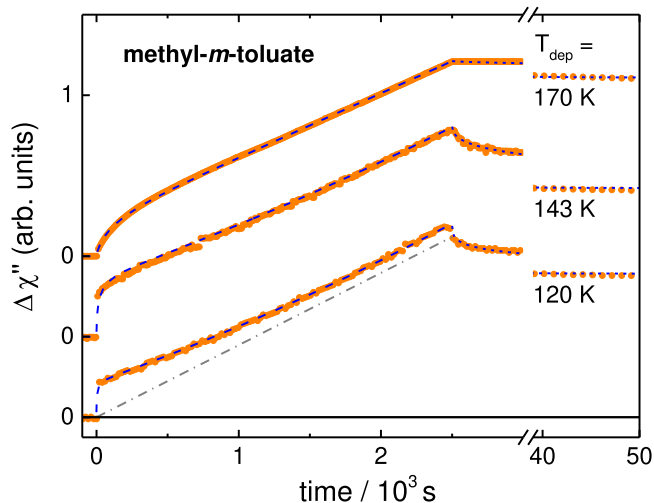
FIG. 4. Three representative deposition curves of MMT, shown in terms of $\Delta\chi''(t)$ for $T_{dep} = 120$, 143, and 170 K (symbols). The dashed lines are fits using the functions outlined in Fig. 5 and the parameters given in Fig. 6. The straight dashed–dotted line is meant to emphasize the curvature of the $T_{dep} = 120$ K case.

time of $t_{dep} = 2500$ s. In each case, the real part of the incremental susceptibility, $\Delta\chi'(t)$, is a linear increase as in Fig. 2, equivalent to a total capacitance change of ≈ 0.2 pF. The appearance of $\Delta\chi''(t)$, however, changes qualitatively with temperature, with a selection of characteristic curves shown in Fig. 4.

In order to quantify the various features of deposition curves, $\Delta\chi''(t)$, such as those in Fig. 4, the following empirical fit function has been employed:
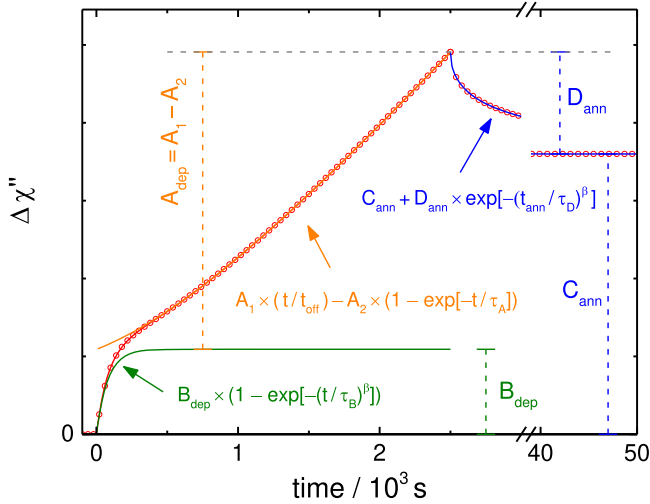
FIG. 5. Definition of functions and parameters involved in the analysis of $\Delta\chi''(t)$ for all ten films deposited between 40 and 170 K, all with deposition rates $r_{dep} \approx 0.092$ nm s^{-1} and film thicknesses $d_{dep} \approx 225$ nm.

FIG. 6. Amplitude parameters of the $\Delta\chi''(t)$ analysis outlined in Fig. 5. The values of A_{dep} and C_{ann} are similar, meaning that the level that remains after 50 000 s (C_{ann}) is almost the same as the near linear build-up during deposition ($A_{dep} = A_1 - A_2$). The values of B_{dep} and D_{ann} are similar, indicating that the drop associated with annealing after deposition (D_{ann}) is related to the amplitude of the initial fast rise (B_{dep}).
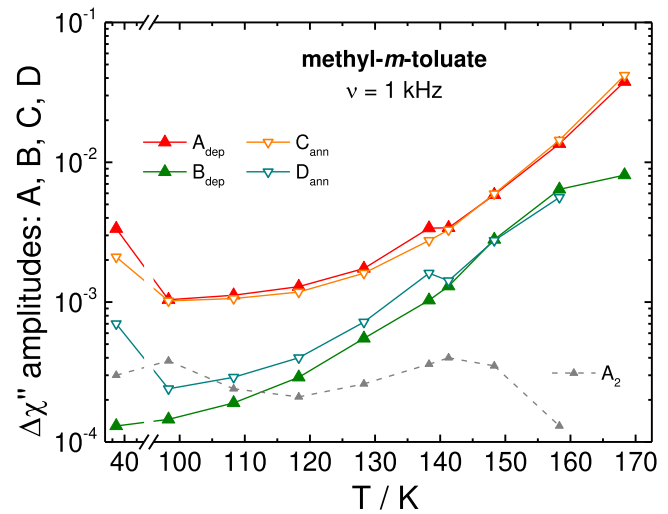
$$\Delta\chi''(t) = A_1 \times \left(\frac{t}{t_{dep}}\right) - A_2 \times \left(1 - e^{-\frac{t}{\tau_A}}\right)$$
$$+ B_{dep} \times \left(1 - e^{-\left(\frac{t}{\tau_B}\right)^\beta}\right). \quad (1)$$

Here, the first and second terms represent the overall near linear rise for $0 \leq t/t_{dep} \leq 1$, where A_2 accounts for a convex curvature with a fixed $\tau_A = 1000$ s. The third term accounts for the initial fast rise, represented by a stretched exponential rise function with a time constant τ_B and an exponent $0.5 < \beta \leq 0.7$. Different terms in Eq. (1) correspond to different layers that are subject to the same electric field, so these terms are additive with respect to χ, as with parallel capacitors. At the end of the deposition process, i.e., at $t = t_{dep}$, the total increase of the loss is approximated (within 1%) by

$$\Delta\chi''(t_{dep}) = A_{dep} + B_{dep} = A_1 - A_2 + B_{dep} = C_{ann} + D_{ann}. \quad (2)$$

During the annealing process after deposition, i.e., for $t > t_{dep}$, the $\Delta\chi''$ signal is observed to drop by the amount D_{ann} to the level of C_{ann}. For clarity, the parameters involved in these fits are schematically outlined in Fig. 5.

The results of these analyses for the $d_{dep} \approx 225$ nm and $r_{dep} \approx 0.092$ nm s^{-1} series of MMT films are compiled vs temperature in Fig. 6, with examples of the fits included in Fig. 4. The obvious features are that $A_{dep} \approx C_{ann}$ and $B_{dep} \approx D_{ann}$, meaning that the amount of total near linear rise ($A_{dep} = A_1 - A_2$) is similar to the amount C_{ann} of $\Delta\chi''$ that remains after a long annealing time and that the amount D_{ann} lost during annealing is associated with the initial fast rise to the level of B_{dep}. It is also visible that the component A_2 (which accounts for the convex curvature of the total rise) remains a small fraction of the amplitude $\Delta\chi''(t_{dep}) = A_{dep} + B_{dep}$ that accumulates during the deposition.
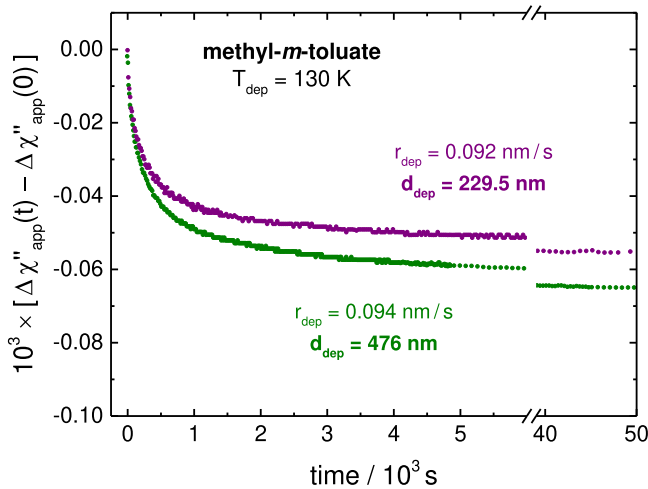
After the initial fast rise, the increase in $\Delta\chi''(t)$ (associated with the amplitude A_{dep}) is not linear in time, although $\Delta\chi'(t)$ shows near perfect linearity (see Fig. 2) for all depositions, indicative of a constant deposition rate r_{dep} for each sample. To clarify the origin of this nonlinear behavior of $\Delta\chi''(t)$, a $d_{dep} = 230$ nm film has been deposited onto the substrate at $T_{dep} = 130$ K at a rate of 0.092 nm s^{-1}, annealed for 5×10^4 s, and another 230 nm film has been deposited under identical conditions onto the annealed one. The resulting $\Delta\chi''(t)$ traces are depicted in Fig. 7 and show very similar behavior. Close scrutiny reveals that the curvature associated with the first film is not discernible for the second film on top. This suggests that the reduced slope of $\Delta\chi''(t)$ after the sharp rise (associated with the amplitude A_2) at the lower temperatures is a matter of proximity to the substrate, which leads to a reduced dielectric susceptibility near the interface. Together with the constant value of τ_A, this suggests a layer with reduced mobility of about 90 nm in thickness near the substrate.

The three $\Delta\chi''(t)$ curves for 120, 143, and 170 K in Fig. 4 suggest a correlation among the amplitudes of the initial fast rise and the respective slow annealing drops observed after deposition. The analysis results shown in Fig. 6 support this quantitatively by observing that $A_{dep} \approx C_{ann}$ for the entire temperature range from 40 to 170 K. Additional support for this notion comes from comparing the annealing behavior of two films, both deposited at $T_{dep} = 130$ K at a rate of $r_{dep} \approx 0.093$ nm s^{-1}, but one with twice the thickness as the other, 476 nm vs 230 nm. Annealing for 5×10^4 s leads to a drop of $\Delta\chi''_{app}(t)$ around 0.06 for both cases; instead of scaling with the film thickness, see Fig. 8. This is consistent with only the surface layer being affected by annealing rather than the bulk of the film.

The time dependence of the annealing process is depicted in Fig. 9 as the normalized reduction of the loss,
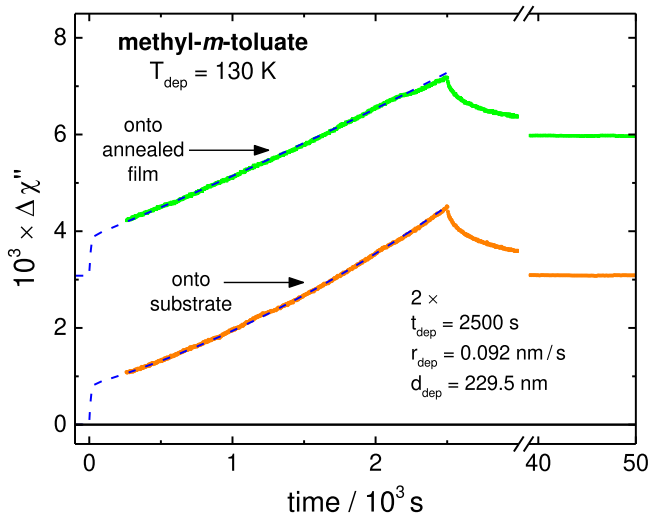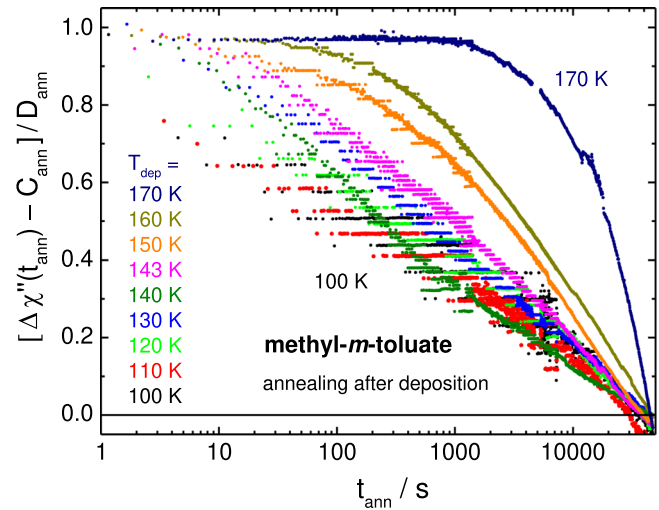
FIG. 7. Deposition of two MMT films, one on top of the other, both with T_{dep} = 130 K, t_{dep} = 2500 s, r_{dep} = 0.092 nm/s, and d = 229.5 nm. Only the film deposited onto the substrate has convex curvature, indicating that $\partial \Delta \chi''/\partial t$ is lower near the substrate relative to 100 nm or more away from the substrate.

FIG. 9. Loss reduction by annealing after the deposition is stopped (t_{ann} = 0), shown in terms of $\Delta \chi''_{norm}(t_{ann}) = [\Delta \chi''(t_{ann}) - C_{ann}]/D_{ann}$, i.e., normalized to unity and zero at short and long times, respectively. The discrete steps of the curves at low temperatures reflect the resolution of the setup: $\tan \delta = 10^{-7}$.

FIG. 8. Annealing curves for two MMT films that differ in thickness by a factor of about 2, but both deposited at T_{dep} = 130 K with $r_{dep} \approx 0.093$ nm/s. The total change of $\Delta \chi''_{app}$ recorded over 50 000 s is quite similar, indicating that it does not scale with the film thickness and is associated with the surface layer.

$[\Delta \chi''(t_{ann}) - C_{ann}]/D_{ann}$ vs logarithmic time. For $T < 150$ K, the half-point is reached after about 300 s, regardless of temperature. At or above 150 K, the times to reach a steady state become longer, and at $T = 170$ K ($= T_g$), the loss continues to decrease significantly at $t_{ann} = 50\,000$ s. This is unexpected because, at $T_g = 170$ K, the material is assumed to equilibrate within about 100 s. This raises the question of whether annealing in this case is confined to the surface layer, to the interfacial layer near the substrate, or to the bulk of the film.

To clarify the origin of the long annealing process at T_g, two films were deposited at $T_{dep} = 170$ K at rates of $r_{dep} \approx 0.094$ nm s^{-1}, one $d_{dep} = 174$ nm film onto the substrate, and a second $d_{dep} = 356$ nm film on top of the annealed first film (see Fig. 10). A similar change in amplitude and decay rate of $\Delta \chi''_{app}$ is observed in the annealing processes of the first and second films, nor do these amplitudes scale with the film thickness difference of a factor of two. Moreover, the two films were deposited on very different substrates: solid borosilicate for the first and the mobile surface layer of the MMT underlayer for the second film. Therefore, we associate this slow process with the material at the surface.
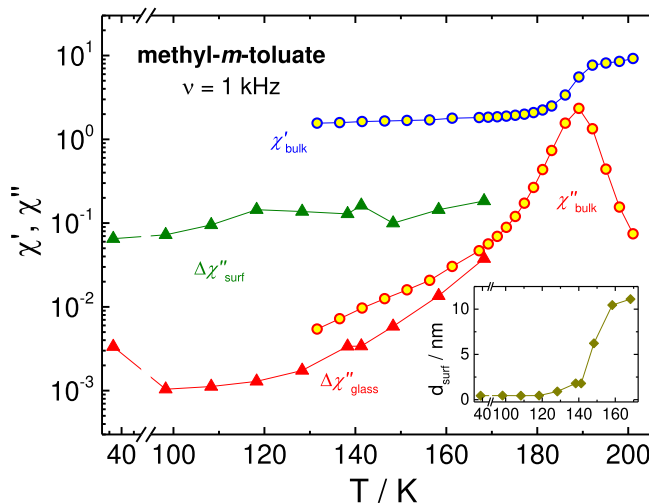
IV. DISCUSSION

Films of MMT with $d_{dep} \approx 225$ nm thickness are compared regarding their dielectric signatures during and after vapor deposition at a rate of $r_{dep} \approx 0.1$ nm s^{-1}, with T_{dep} being varied from 40 to 170 K. The real component, $\Delta \chi'$, is used to gauge film thickness, d_{dep}, and deposition rate, r_{dep}. The loss component, $\Delta \chi''$, is understood to reflect the fictive temperature, T_{fic}, of the material via the dynamics, as dipole density remains practically constant in the present experimental range. The quantity T_{fic} is understood to represent the temperature at which a given property X of the equilibrium system, $X_{eq}(T_{fic})$, is expected to resemble that of the non-equilibrium state in question, i.e., $X_{eq}(T_{fic}) \approx X_{non-eq}(T)$. The in situ monitoring of $\Delta \chi''(t)$ during deposition and the analysis of the resulting curves provide a detailed picture of the film dynamics. According to the examples in Fig. 4, there is a fast initial rise of $\Delta \chi''(t)$ characterized by the parameters B_{dep}, τ_B, and β, followed by a near linear rise with amplitude $A_{dep} = A_1 - A_2$. The magnitude of A_{dep} is practically equal to the level C_{ann} that remains after sufficiently long annealing (see Fig. 6), consistent with assigning these values to the bulk of the film and with the high kinetic stability of these glasses.
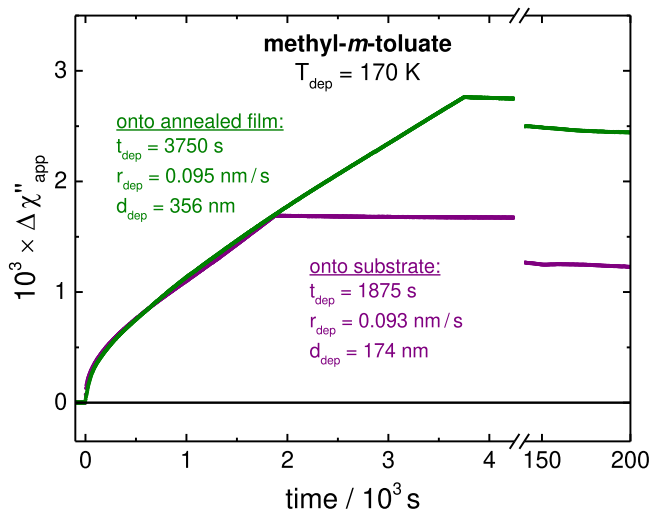
FIG. 10. Deposition and annealing curves for two MMT films that differ in thickness by a factor of about 2, but both deposited at T_{dep} = 170 K with $r_{dep} \approx 0.094$ nm/s, and the thicker one deposited on top of the thinner one. The total change of $\Delta\chi''_{app}$ during annealing over 200 000 s is quite similar, indicating that it does not scale with the film thickness and is associated with the surface layer instead of with the bulk of the film or the layer at the substrate.


FIG. 11. Susceptibilities χ' and χ'' of MMT cooled from the melt (open circles, taken from Ref. 29), compared with $\Delta\chi''$ of the vapor deposited films. The value of $\Delta\chi''_{glass}$ is determined by $A_{dep} = A_1 - A_2$, and that of $\Delta\chi''_{surf}$ by $B_{dep} \times d_{dep}/d_{surf}$, with $d_{surf} = \tau_B \times r_{dep}$ representing the average surface layer thickness. See the inset for a graph of d_{surf} vs T_{dep}, and note that τ_B changes proportionally.

An overview of the loss behavior for the bulk of the glassy film and of the surface layer is provided in Fig. 11, which compares the present results with those for MMT cooled from the melt and labeled as χ'_{bulk} and χ''_{bulk}. According to Fig. 11, the χ'_{bulk} of MMT is nearly temperature invariant in the glassy state, so a linear rise of $\Delta\chi'$ as in Fig. 2 is expected for a constant deposition rate r_{dep}, even if the fictive temperature changes in the course of the deposition. The value, $\Delta\chi''_{glass}$, for the bulk of the vapor deposited films, is equal to the value of A_{dep} in the analysis described earlier, cf. Fig. 5 and Eq. (1). The results compiled in Fig. 11 show that the bulk of the film has $\Delta\chi''_{glass} < \chi''_{bulk}$, consistent with the lower fictive temperatures of the as-deposited films relative to melt cooled MMT. The rise of $\Delta\chi''_{glass}$ for $T \approx 40$ K is a common feature of molecular glasses and is typically associated with the transition dynamics within two-level systems.[30] In order to obtain a corresponding average value for the surface layer, $\Delta\chi''_{surf}$, a value for the thickness of the surface layer, d_{surf}, is required. It is estimated from the characteristic time of the initial fast rise, τ_B in Eq. (1), in relation to the deposition rate, i.e., $d_{surf} = \tau_B \times r_{dep}$. As shown in the inset of Fig. 11, d_{surf} rises sharply from at or below resolution to about 10 nm at $T = 170$ K. Note that τ_B changes with T_{dep} in the same manner, as r_{dep} is practically constant. With d_{surf} known, $\Delta\chi''_{surf}$ can be determined from the amplitude of the initial rise, B_{dep}, by scaling up according to the volume fraction of the surface layer, $\Delta\chi''_{surf} = B \times d_{dep}/d_{surf}$. It can be observed that the loss of the surface layer remains near $\Delta\chi''_{surf} \approx 0.1$ for all temperatures 40 K $\leq T \leq$ 170 K, a level equivalent to a fictive temperature near or somewhat above T_g.

Within the deposition curves, $\Delta\chi''(t)$, the signature of the fast surface layer is seen as the more rapid rise of the loss during the initial phase of the deposition (see Fig. 4). For all temperatures, this indicates high surface mobility regarding dipole reorientation within a thin layer that remains at the surface of the film. A more detailed

picture can be obtained from the fits based on Eq. (1) and the resulting parameters by calculating the position-dependent dielectric loss via the time derivative of $\Delta\chi''(t)$, provided that the film thickness increases linearly with time, which is confirmed by all $\Delta\chi'_{app}(t)$ curves. The calculation for this derivative yields

$$\frac{\partial \Delta\chi''(t)}{\partial t} = \frac{A_1}{t_{dep}} - \frac{A_2}{\tau_A} \times e^{-\frac{t_{dep}-t}{\tau_A}} + B_{dep} \times \frac{\beta}{t}\left(\frac{t}{\tau_B}\right)^\beta e^{-\left(\frac{t}{\tau_B}\right)^\beta}. \quad (3)$$

This expression represents the susceptibility density per unit time t or per unit thickness d, since d is proportional to t. Rescaling to values equivalent to $\Delta\chi''$ of a completely filled capacitor is accomplished by multiplying with t_{dep} so that the quantity of interest is $\partial\Delta\chi''(t)/\partial t \times t_{dep}$ vs $d = r_{dep} \times t$. The resulting curves are shown in Fig. 12 on a logarithmic scale for position $\delta = d_{dep} - d$ so that the surface is at $\delta = 0$ and the substrate at $\delta \approx 200$ nm. The downturn in the 150 nm $\leq \delta \leq$ 200 nm range is the result of the lower $\Delta\chi''$ vs t slope in the first 1000 s (=τ_A), seen as slight convex curvature in Figs. 4 and 7 with an amplitude quantified by A_2. This feature disappears as T_{dep} approaches T_g from below. Proximity within about 90 nm (=$d_{dep} \times \tau_A/t_{dep}$) of the borosilicate substrate is assumed to be responsible for these lower $\Delta\chi''$ values, which could be a consequence of reduced mobility of MMT for the present deposition conditions.

Regarding the surface dynamics, Fig. 12 shows that $\Delta\chi''$ for $\delta \leq 1$ nm rises a factor of about 10 above the level of the bulk of the glass (10 nm $\leq \delta \leq$ 100 nm) and that $\Delta\chi''$ immediately at the surface (see $\delta < 1$ nm range in Fig. 12) increases with temperature. Note that the less temperature-dependent value of $\Delta\chi''_{surf}$ in Fig. 11 is an average over the layer thickness $d_{surf}(T)$. Qualitatively, such a decoupling of the surface layer behavior from the film dynamics had also been observed by Zhang and Fakhraai,[9] who saw high surface mobility
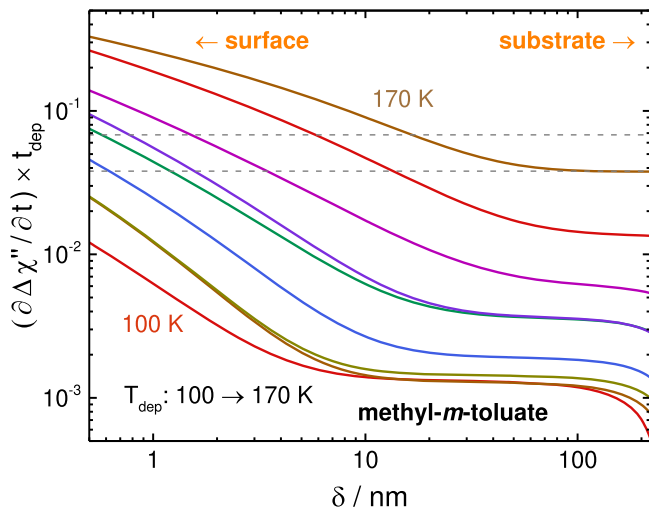
FIG. 12. Position dependent susceptibility across the film thickness of about 200 nm, determined from the fits to the deposition curves as $\partial\Delta\chi''(t)/\partial t \times t_{dep}$, with $t_{dep} = 2500$ s in all cases. The quantity δ gauges the depth below the surface at $\delta = 0$, so the substrate is at $\delta \approx 200$ nm. The lower dashed line indicates the equilibrium level at $T_g = 170$ K; the upper one is the level of χ'' equivalent to a relaxation time of $\tau_\alpha = 5$ s, the approximate time to deposit a monolayer of MMT at the present $r_{dep} \approx 0.1$ nm s^{-1}.
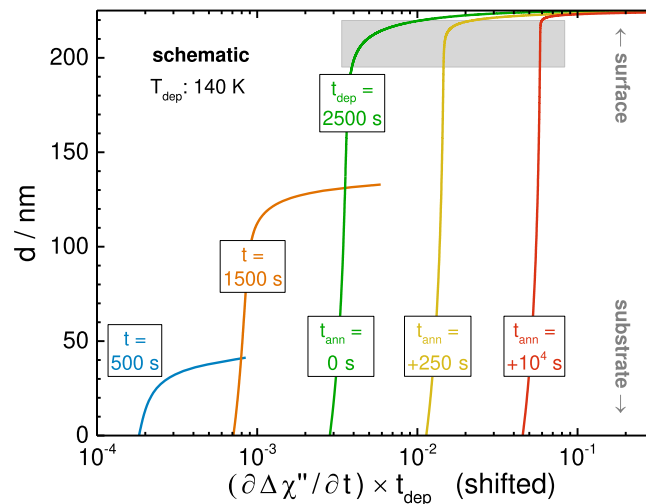
FIG. 13. Position dependent susceptibility across the film thickness of 225 nm for the case of $T_{dep} = 140$ K. The center curve labeled $t_{dep} = 2500$ s and $t_{ann} = 0$ s represents the $T_{dep} = 140$ K case of Fig. 12, but now on swapped scales: linear d vs logarithmic $\partial\Delta\chi''(t)/\partial t \times t_{dep}$. The remaining curves are not experimental data but rather derived from Eq. (3). The two curves on the left are the profiles expected after $t = 500$ and 1500 s of deposition, assuming that the more mobile layers remain on top. The two curves on the right represent curves after $t_{ann} = 250$ and 10^4 s of annealing, consistent with the $T_{dep} = 140$ K data in Fig. 9. With the exception of the center curve ($t_{dep} = 2500$ s), lines are spaced by factors of 4 on the abscissa scale for clarity. The shaded area indicates the d-range associated with the bulk of the changes observed during annealing, i.e., 5–30 nm below the surface.

relative to the film below with a reduced temperature dependence compared with the α-relaxation of the liquid state.

Based on these $\Delta\chi''$ data, deposition temperatures above 140 K ($\approx 0.8 T_g$) lead to surface dynamics where the top mono-layer (≈ 0.3 nm) can relax prior to the 5 s it takes to become buried at the present deposition rate of $r_{dep} \approx 0.1$ nm s^{-1}. The loss level equivalent to this 5 s criterion is indicated by the top dashed line in Fig. 12. As $\Delta\chi''$ at the surface increases with temperature, molecules will be able to sample phase space more effectively in the time they remain in proximity to the surface and thus form a structure that is close to the equilibrium glassy state. Naturally, the time molecules remain near the surface will depend on the deposition rate, r_{dep}. In addition, evident from Fig. 12 is the continuous change of $\Delta\chi''$ from the surface ($\delta \leq 1$ nm) to the bulk (10 nm $\leq \delta \leq$ 100 nm) level, inconsistent with a simple two layer picture with a sharp boundary between surface and bulk behavior.

All samples display considerable annealing behavior after the deposition is terminated. The observation that $A_{dep} \approx C_{ann}$ and $B_{dep} \approx D_{ann}$ in Fig. 11 as well as the findings from stacked films in Figs. 8 and 10 all indicate that annealing is solely associated with the surface layer. This notion is compatible with the very different values of τ_B and τ_D, as τ_B is determined by d_{surf} (via r_{dep}) while τ_D reflects annealing dynamics. In the temperature range in which vapor deposition leads to kinetically stable glasses, $0.75 T_g \leq T_{dep} \leq 0.9 T_g$, the surface layer has almost reached a steady state within the deposition time $t_{dep} = 2500$ s, and a considerable change has already occurred in the first 250 s (see Fig. 9). For these cases with $T_{dep} < 145$ K, the volume fraction of the surface layer does not exceed 1%, and annealing in this range of T_{dep} has little influence on the overall film behavior. Moreover, D_{ann} is about 40% higher than B_{dep} in this range (see

Fig. 6), meaning that the more mobile material can relax further if given time in excess of $t_{dep} = 2500$ s.

It may appear contradictory that the "fast" surface layer displays changes in $\Delta\chi''(t_{ann})$ beyond 10 000 s after the deposition process. The explanation rests on the continuous change of $\Delta\chi''$ with increasing depth below the surface, as illustrated in Fig. 13 for the $T_{dep} = 140$ K case. A plausible scenario for the observed deposition curves, $\Delta\chi''(t)$, is that the surface layer moves away from the substrate as the glassy film grows in thickness below; see the three leftmost curves in Fig. 13. Beyond the end of the deposition process at $t = 2500$ s and $t_{ann} = 0$, the lower and less mobile part of the surface layer slowly tends toward equilibrium, while the top layer remains mobile. This is indicated by the three rightmost curves in Fig. 13, with the shaded area indicating that most of the change of $\Delta\chi''(t_{ann})$ observed in the course of annealing is believed to occur between 5 and 30 nm below the surface.

With increasing deposition temperature, the surface layer becomes thicker, cf. inset Fig. 11, reaching more than 10 nm into the film at $T_g = 170$ K. Correlated with this rapid thickness increase for $T_{dep} \geq 150$ K is the strongly retarded annealing behavior seen in Fig. 9, again occurring only within the mobile layer near the surface. A potential explanation for the increasing annealing time for temperatures above $T = 150$ K is that a higher volume fraction of not yet equilibrated MMT is buried relatively deep below the surface layer, leading to longer annealing times. That there is any annealing beyond times of $\tau_\alpha = 100$ s at $T_g = 170$ K is unexpected and surprising. Without further evidence, it can only be speculated that the

surface layer of vapor-deposited MMT has a different structure than melt-cooled MMT at T_g, and its conversion to the ordinary liquid structure is responsible for the slow change of $\Delta\chi''$ after deposition, analogous to Fig. 13, but with the mobile layer initially reaching much further below the surface.

It is useful to compare our findings to previous reports of surface mobility for low-molecular-weight glassformers. The finding that surfaces are highly mobile, even below T_g, is qualitatively consistent with previous measurements of surface diffusion.[8,9,31] The surface equilibration mechanism successfully uses the idea of highly mobile surfaces to explain how the stability of PVD glasses depends on substrate temperature and deposition rate.[6] The surface equilibration mechanism has also been used to explain anisotropy in PVD glasses and includes the idea that orientation that is preferred at the free surface during deposition can be altered by mobility just below the surface if the deposition is performed at a low enough rate.[20,32,33] These PVD experiments are qualitatively consistent with the extended gradient of mobility shown in Fig. 12, as are surface diffusion measurements with molecules that extend below the free surface to various depths.[10] Our present work shows that an extremely long time is required for the near-surface dynamics to age to equilibrium, even for deposition at T_g. While this is surprising, given that we expected the entire film to equilibrate in ~100 s, we know of no experimental results that contradict this. This is clearly an area where complementary experiments would be helpful. Analogous experiments on other molecular glasses, including those with varying kinetic stability, would help to identify whether the presently observed features are material-specific or not.

V. SUMMARY AND CONCLUSIONS

Glasses have been prepared by vapor deposition using methyl-*m*-toluate (MMT), a polar glass forming molecular material with a glass transition temperature $T_g = 170$ K. Films of about 200 nm thickness have been deposited at rates of 0.1 nm/s onto a borosilicate substrate with deposition temperatures between 40 and 170 K. MMT is known to form kinetically highly stable glasses at or near $0.85T_g = 145$ K, and it is simple in the sense that vapor-deposited glasses recover the properties of the melt-cooled liquid if warmed above T_g.

During and after deposition, the dielectric permittivity of MMT films has been measured with a resolution of $\tan\delta = 10^{-7}$ via an interdigitated electrode structure with a geometric capacitance of 2.2 pF. In all cases, the capacitance of the cell rose linearly with time, indicative of a constant deposition rate. During deposition, the dielectric loss of the film rises quickly at first and then nearly linearly with time. The analysis of these deposition curves reveals slightly different dynamics near the substrate, a bulk of the film that does not change the loss behavior for 50 000 s after deposition, and a surface layer of more mobile material. The thickness of this layer is at or below 1 nm for deposition at low temperatures and sharply rises to above 10 nm average thickness at T_g. The dielectric loss, understood as an indicator of the fictive temperature T_{fic}, is observed to change gradually from the mobile surface with $T_{fic} > T_g$ to the much lower value of the stable glass, where T_{fic} is assumed to be close to the deposition temperature. After the deposition is stopped, this mobile surface layer undergoes a considerable reduction in its dielectric loss, and this annealing effect is believed to arise

from material positioned 5–30 nm below the surface. The picture of a fictive temperature gradient near the surface as derived from these observations differs from that of a distinct mobile layer that quickly and directly converts to the kinetically stable glass. Moreover, the post-deposition annealing behavior observed here suggests that the surface layer thickness determined long after deposition may not reflect the situation during deposition. This *in situ* application of high resolution dielectric relaxation techniques during and after physical vapor deposition is capable of providing additional information for improving our understanding of materials obtained by physical vapor deposition.

AUTHOR DECLARATIONS

Conflict of Interest

The authors have no conflicts to disclose.

Author Contributions

R. Richert: Conceptualization (equal); Formal analysis (lead); Funding acquisition (equal); Investigation (lead); Writing – review & editing (equal). **M. E. Tracy**: Conceptualization (equal); Writing – review & editing (equal). **A. Guiseppi-Elie**: Resources (supporting); Writing – review & editing (supporting). **M. D. Ediger**: Conceptualization (equal); Funding acquisition (equal); Writing – review & editing (equal).

DATA AVAILABILITY

The data that support the findings of this study are available from the corresponding author upon reasonable request.

REFERENCES

[1] S. F. Swallen, K. L. Kearns, M. K. Mapes, Y. S. Kim, R. J. McMahon, M. D. Ediger, T. Wu, L. Yu, and S. Satija, "Organic glasses with exceptional thermodynamic and kinetic stability," Science **315**, 353 (2007).

[2] L. Berthier and M. D. Ediger, "Facets of glass physics," Phys. Today **69**(1), 40 (2016).

[3] K. Dawson, L. A. Kopff, L. Zhu, R. J. McMahon, L. Yu, R. Richert, and M. D. Ediger, "Molecular packing in highly stable glasses of vapor-deposited tris-naphthylbenzene isomers," J. Chem. Phys. **136**, 094505 (2012).

[4] M. D. Ediger, "Perspective: Highly stable vapor-deposited glasses," J. Chem. Phys. **147**, 210901 (2017).

[5] Y. Z. Chua, M. Ahrenberg, M. Tylinski, M. D. Ediger, and C. Schick, "How much time is needed to form a kinetically stable glass? AC calorimetric study of vapor-deposited glasses of ethylcyclohexane," J. Chem. Phys. **142**, 054506 (2015).

[6] M. S. Beasley, C. Bishop, B. J. Kasting, and M. D. Ediger, "Vapor-deposited ethylbenzene glasses approach 'ideal glass' density," J. Phys. Chem. Lett. **10**, 4069 (2019).

[7] C. W. Brian and L. Yu, "Surface self-diffusion of organic glasses," J. Phys. Chem. A **117**, 13303 (2013).

[8] L. Yu, "Surface mobility of molecular glasses and its importance in physical stability," Adv. Drug Delivery Rev. **100**, 3 (2016).

[9] Y. Zhang and Z. Fakhraai, "Decoupling of surface diffusion and relaxation dynamics of molecular glasses," Proc. Natl. Acad. Sci. U. S. A. **114**, 4915 (2017).

[10] Y. Li, W. Zhang, C. Bishop, C. Huang, M. D. Ediger, and L. Yu, "Surface diffusion in glasses of rod-like molecules posaconazole and itraconazole: Effect of interfacial molecular alignment and bulk penetration," Soft Matter **16**, 5062 (2020).

[11] R. C. Bell, H. Wang, M. J. Iedema, and J. P. Cowin, "Nanometer-resolved interfacial fluidity," J. Am. Chem. Soc. **125**, 5176 (2003).

[12] S. Napolitano, E. Glynos, and N. B. Tito, "Glass transition of polymers in bulk, confined geometries, and near interfaces," Rep. Prog. Phys. **80**, 036602 (2017).

[13] N. G. Perez-de-Eulate, V. Di Lisio, and D. Cangialosi, "Glass transition and molecular dynamics in polystyrene nanospheres by fast scanning calorimetry," ACS Macro Lett. **6**, 859 (2017).

[14] C. W. Brian, L. Zhu, and L. Yu, "Effect of bulk aging on surface diffusion of glasses," J. Chem. Phys. **140**, 054509 (2014).

[15] J. D. Stevenson and P. G. Wolynes, "On the surface of glasses," J. Chem. Phys. **129**, 234514 (2008).

[16] S. Samanta, G. Huang, G. Gao, Y. Zhang, A. Zhang, S. Wolf, C. N. Woods, Y. Jin, P. J. Walsh, and Z. Fakhraai, "Exploring the importance of surface diffusion in stability of vapor-deposited organic glasses," J. Phys. Chem. B **123**, 4108 (2019).

[17] S. Singh and J. J. de Pablo, "A molecular view of vapor deposited glasses," J. Chem. Phys. **134**, 194903 (2011).

[18] L. Berthier, P. Charbonneau, E. Flenner, and F. Zamponi, "Origin of ultrastability in vapor-deposited glasses," Phys. Rev. Lett. **119**, 188002 (2017).

[19] C. Bishop, Y. Li, M. F. Toney, L. Yu, and M. D. Ediger, "Molecular orientation for vapor-deposited organic glasses follows rate-temperature superposition: The case of posaconazole," J. Phys. Chem. B **124**, 2505 (2020).

[20] S. S. Dalal, D. M. Walters, I. Lyubimov, J. J. de Pablo, and M. D. Ediger, "Tunable molecular orientation and elevated thermal stability of vapor-deposited organic semiconductors," Proc. Natl. Acad. Sci. U. S. A. **112**, 4227 (2015).

[21] H.-B. Yu, M. Tylinski, A. Guiseppi-Elie, M. D. Ediger, and R. Richert, "Suppression of β relaxation in vapor-deposited ultrastable glasses," Phys. Rev. Lett. **115**, 185501 (2015).

[22] C. Rodríguez-Tinoco, M. Rams-Baron, K. L. Ngai, K. Jurkiewicz, J. Rodríguez-Viejo, and M. Paluch, "Secondary relaxation in ultrastable etoricoxib: Evidence of correlation with structural relaxation," Phys. Chem. Chem. Phys. **20**, 3939 (2018).

[23] B. J. Kasting, M. S. Beasley, A. Guiseppi-Elie, R. Richert and M. D. Ediger, "Relationship between aged and vapor-deposited organic glasses: Secondary relaxations in methyl-*m*-toluate," J. Chem. Phys **151**, 144502 (2019).

[24] A. R. Young-Gonzales, A. Guiseppi-Elie, M. D. Ediger, and R. Richert, "Modifying hydrogen-bonded structures by physical vapor deposition: 4-methyl-3-heptanol," J. Chem. Phys. **147**, 194504 (2017).

[25] J. P. Gabriel, B. Riechers, E. Thoms, A. Guiseppi-Elie, M. D. Ediger, and R. Richert, "Polyamorphism in vapor-deposited 2-methyltetrahydrofuran: A broadband dielectric relaxation study," J. Chem. Phys. **154**, 024502 (2021).

[26] J. P. Gabriel, E. Thoms, A. Guiseppi-Elie, M. D. Ediger, and R. Richert, "A liquid with distinct metastable structures: Supercooled butyronitrile," J. Chem. Phys. **156**, 044501 (2022).

[27] B. Riechers, A. Guiseppi-Elie, M. D. Ediger, and R. Richert, "Ultrastable and polyamorphic states of vapor-deposited 2-methyltetrahydrofuran," J. Chem. Phys. **150**, 214502 (2019).

[28] L. Yang, A. Guiseppi-Wilson, and A. Guiseppi-Elie, "Design considerations in the use of interdigitated microsensor electrode arrays (IMEs) for impedimetric characterization of biomimetic hydrogels," Biomed. Microdevices **13**, 279 (2011).

[29] A. I. Nielsen, T. Christensen, B. Jakobsen, K. Niss, N. B. Olsen, R. Richert, and J. C. Dyre, "Prevalence of approximate $\sqrt{t}$ relaxation for the dielectric α process in viscous organic liquids," J. Chem. Phys. **130**, 154508 (2009).

[30] C. Hansen and R. Richert, "Dipolar dynamics of low-molecular-weight organic materials in the glassy state," J. Phys.: Condens. Matter **9**, 9661 (1997).

[31] E. Thoms, J. P. Gabriel, A. Guiseppi-Elie, M. D. Ediger, and R. Richert, "*In situ* observation of fast surface dynamics during the vapor-deposition of a stable organic glass," Soft Matter **16**, 10860 (2020).

[32] P. Luo and Z. Fakhraai, "Surface-mediated formation of stable glasses," Annu. Rev. Phys. Chem. **74**, 361 (2023).

[33] I. Lyubimov, L. Antony, D. M. Walters, D. Rodney, M. D. Ediger, and J. J. de Pablo, "Orientational anisotropy in simulated vapor-deposited molecular glasses," J. Chem. Phys. **143**, 094502 (2015).

21 January 2024 08:18:49